Applied Physics A (2021) 127:808
https://doi.org/10.1007/s00339-021-04957-0

Applied Physics A
Materials Science & Processing

Nanocomposite Bi/TiO_2 multilayer thin films deposited by a crossed beam laser ablation configuration

L. A. Martínez-Chávez[1] · K. Esquivel[1] · D. A. Solis-Casados[2] · R. Velázquez-Castillo[1] · E. Haro-Poniatowski[3] · L. Escobar-Alarcón[4]

Received: 16 July 2021 / Accepted: 24 September 2021 / Published online: 3 October 2021

Abstract

A crossed beam pulsed laser deposition configuration was used to prepare nanocomposites Bi/TiO_2 thin films on two different substrates. The multilayered system was formed by depositing TiO_2 and Bi layers alternately. In order to embed the Bi nanostructures in TiO_2, the subsequent TiO_2 layers were synthesized using a constant number of laser pulses (3000) corresponding to a thickness of approximately 21 nm. The Bi nanostructures were deposited on the TiO_2 layers alternately by irradiating the Bi target with 30, 100, 200, and 300 laser pulses. In this way, the Bi nanostructures were embedded inside the TiO_2 matrix. A total of 8 samples with bismuth and one reference, with TiO_2 only, were produced. Transmission Electron Microscopy (TEM) showed that nearly spherical nanoparticles (NPs) were obtained at lower number of pulses, whereas at 300 pulses a quasi-percolated nanostructured Bi film was obtained. X-Ray Photoelectron Spectroscopy (XPS) revealed that the TiO_2 layers were not affected due to the bismuth presence. Raman Spectroscopy showed vibrational features characteristic of the rutile phase for the titania layer. The Raman spectrum of the multilayer prepared using 300 laser pulses on the bismuth, suggests that the Bi layer is formed by a mixture of metallic Bi, and α-Bi_2O_3. The Ultraviolet–Visible Spectroscopy reveals that no substantial changes are presented in the transmittance spectra indicating similar optical properties of the different deposits. Finally, the photoluminescence emission spectra indicate that the substrate position in the deposition chamber affects the electronic structure of the material.

Keywords Nanocomposites · Titanium oxide · Laser ablation · Multilayers

1 Introduction

Nanocomposite materials have become an intense subject of investigation in the last three decades due to their potential applications in various fields such as photocatalysis, plasmonics, energy conversion devices among others [1, 2]. Nanocomposites in thin film-form also have a wide range of applications in particular due to their potential to be used as layers or coatings [3, 4]. These films can be produced by several methods from conventional deposition (thermal evaporation, sputtering), pulsed laser deposition to sol-gel techniques. In the case of semiconductors in thin-film form, these are growing as promising photocatalysts for environmental remediation because they have several advantages over their counterparts in powder or slurry form. For example, their relatively cost-effective due to the reduction in material usage avoids the cost-recycling and recollection after degradation, carry less physical impairment, simply tuning of its material properties, and provides

✉ K. Esquivel
karen_esq_2001@yahoo.com

✉ L. Escobar-Alarcón
luis.escobar@inin.gob.mx

1 División de Investigación y Posgrado, Facultad de Ingeniería, Universidad Autónoma de Querétaro, Cerro de Las Campanas, C.P. 76010 Santiago de Querétaro, Qro, México

2 Facultad de Química, Universidad Autónoma del Estado de México, Paseo Colon Esq. Paseo Tollocan S/N, CP 50120 Toluca, Estado de México, México

3 Departamento de Física, Universidad Autónoma Metropolitana Iztapalapa, Apdo. Postal 55-534 Ciudad de México, CDMX, México

4 Departamento de Física, Instituto Nacional de Investigaciones Nucleares, Carr. México-Toluca S/N, La Marquesa, C.P. 52750 Ocoyoacac, Edo. de México, México

the miniaturization possibility of devices [5]. TiO_2 is an important semiconductor in photocatalysis due to its strong oxidizing power and non-toxicity [6]. However, its major limitations as photocatalyst are the high recombination rate of the electron–hole pairs produced under light irradiation at or near its surface, and it is only active under UV light irradiation [7]. Several strategies have been proposed to overcome these issues, such as modifying the TiO_2 by doping with metals and nonmetals, co-doping with nonmetals, semiconductors coupling, and bandgap modification by creating oxygen vacancies and oxygen sub-stoichiometry, to mention a few [8]. Therefore, it becomes very important to investigate thin film deposition alternatives to grow composite nanomaterials formed by two oxides as well as of oxides modified with metals as dopants or as embedded nanoparticles to obtain semiconductors with better photocatalytic properties. The Pulsed Laser Deposition (PLD) technique has been widely employed because it is very useful for thin film deposition of oxides even with complex compositions [9]. Among the advantages of this technique, it is worth mentioning the presence of ions and other excited species with high kinetic energy, typically from tens to hundreds of eV as well as its very high plasma density resulting in materials with superior properties compared with the films deposited using other techniques [10]. Additionally, its versatility allows to combine it with other deposition techniques [11, 12] as well as to use configurations combining several ablation plasmas [13, 14]. Particularly, the deposition using two independent plasmas produced from different targets giving the possibility to vary the plasma parameters independently and in a controlled manner. In this way, multilayer films [15] and nanocomposite films consisting of either semiconductor or metal nanocrystals embedded in a dielectric host [16] have been prepared. Another advantage of PLD is the possibility to grow nanoparticles in vacuum [17] or in presence of an ambient gas [18] in a straightforward way such as Bi nanoparticles [19, 20]. Finally, the preparation of thin films of oxides modified with metals using alternative configurations of laser ablation has been successfully implemented and employed in our research group to obtain Co:TiO_2 [21], Bi:TiO_2 [22], V_2O_5:Ag [23], TiO_2:Zn [14] and Au:TiO_2 multilayer thin films [24], with reasonable control of the composition as well as an excellent photocatalytic response under simulated solar irradiation. It is worth mentioning that in the case of Bi embedded in different matrices such as amorphous Ge or Al_2O_3 interesting thermo-optical properties have been reported [25, 26]. These are due to the fact that Bi has a low melting point and optical changes involving phase transitions can be easily detected opening the possibility of developing thermo-optical switches among other applications [27]. In this work taking into account the potential applications in photocatalysis and more recently in thermo-optics, we have fabricated multilayered structures of Bi/TiO_2 by pulsed laser deposition. The characterization was done by Raman, X-ray Photoelectron, and UV–Vis Spectroscopies as well as Transmission Electron Microscopy, Photoluminescence and the corresponding results are presented and analyzed.

2 Experimental procedure

2.1 Thin films preparation

Bi/TiO_2/Bi/…/TiO_2/Bi/TiO_2 multilayer thin films were prepared by the Pulsed Laser Deposition (PLD) technique using a crossed beam deposition configuration which is shown in Fig. 1. The laser ablation system used in this work consisted of a vacuum chamber evacuated by a turbomolecular pump to a base pressure close to 8×10^{-6} Torr. In order to obtain the stacking sequence of Bi on TiO_2, two laser beams were used to ablate alternatively two targets, TiO_2 and Bi (99.99% purity with 2.54 cm diameter and 0.63 cm thickness), positioned perpendicularly to each other. Laser ablation was performed using an Nd:YAG laser with emission at the second harmonic (532 nm) and a 5 ns pulse duration, working at a 10 Hz repetition rate. The TiO_2 plasma was generated by a laser fluence close to 26.0 J/cm^2 (energy per pulse = 100 mJ, spot size = 0.7 mm), whereas the Bi plasma was produced using a fluence close to 1.8 J/cm^2 (energy per pulse = 14 mJ, spot size = 1.0 mm). These ablation conditions were chosen based on previous works [28, 29]. Thin films were deposited onto glass substrates (~6.2 cm^2) placed in two different positions as is seen in Fig. 1a, substrate 1 (S1) was located approximately at 45° with respect to the lines of propagation of the plasmas; substrate 2 (S2) was parallel to the Bi plasma propagation line, the target to substrate distance was 4.2 cm for S1 and 5 cm for S2. The characterization of laser ablation plasmas using Langmuir probes has shown that the angular distributions of the ion density and the ion energy depend strongly on the angle with respect to the normal of the target surface, that is, along the direction of plasma propagation; these plasma parameters reach their maximum values close to the normal and fall sharply when increasing the angle with their minimum values close to 50°, that is, in a direction almost parallel to the plasma propagation line [30]. Consequently, a different material´s growth for each of the substrate positions is expected. This setup was used firstly in order to prepare titanium oxide thin films modified with different Bi content in the same experiment. Secondly, to investigate the probable differences in their optical and structural properties. The multilayer structure was obtained as follows: a) the deposition started with the TiO_2 ablation plasma for 30 min; (ii) afterward, the laser beam on the TiO_2 target was blocked using an external mechanical shutter and the bismuth ablation plasma was produced using different

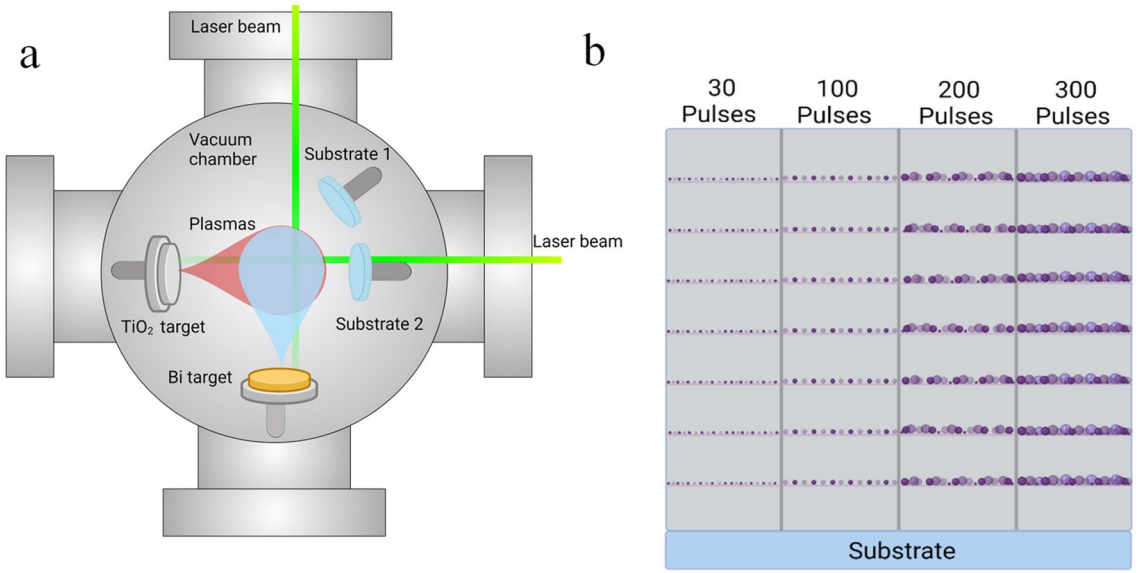

Fig. 1 **a** Experimental setup for multilayer thin film deposition on substrates placed at different positions, **b** Schematic of the multilayer configuration prepared

number of pulses: 30, 100, 200, and 300, respectively; (iii) then the laser beam on the Bi target was blocked, and the ablation of the TiO_2 target was started again for 5 min. This procedure was repeated seven times to obtain 7 Bi/TiO_2 bilayers in 8 different samples, as is schematically shown in Fig. 1b. After deposition, the films were subjected to a thermal treatment at 450 °C for one hour in air. This thermal treatment promotes the transformation of the initially amorphous TiO_2 to its crystalline phase [31].

2.2 Thin films characterization

In order to characterize the bismuth layers, these were deposited directly onto TEM carbon-coated grids and observed in a JEOL 2100 transmission electron microscope. The microstructure of the films was characterized by Raman spectroscopy; the spectra were obtained using a micro-Raman LabRam 800 system, equipped with a confocal microscope Olympus BX40 and a 100X objective; the samples were excited using the second harmonic of an Nd:YAG laser (532 nm). Optical measurements were performed on a Perkin Elmer Lambda 35 UV–Vis spectrophotometer to obtain the transmittance spectra of the films from 200 to 1100 nm. Photoluminescence properties from the thin films were studied by PL spectroscopy using a spectrofluorometer (FluoroMax 4, Horiba Jobyn Ivon) equipped with a 150 W Xenon lamp as an excitation source. X-ray photoelectron spectroscopy (XPS) was used to determine the elemental composition and the chemical bonding of the present elements in the samples. XPS spectra were acquired in the low- and high-resolution regimes with a K-alpha Thermo Scientific XPS spectrometer. The adventitious carbon peak at 284.8 eV was used as the internal standard to compensate for sample charging. All measurements were made in an ultra-high vacuum (UHV) chamber at pressures between 5×10^{-9} and 2×10^{-8} Torr. Etching for XPS measurements under the surface of the films was performed using 1 keV Ar ions with a current density of 10 μA/cm^2.

3 Results and discussion

3.1 TEM characterization of bismuth layers

The morphology of the Bi layers at the different number of laser pulses used to ablate the Bi target was investigated by Transmission Electron Microscopy (TEM). Representative TEM images of the Bi nanostructures obtained at 30, 100, 200, and 300 pulses are shown in Fig. 2. As it is observed in Fig. 2a, the sample prepared using 30 pulses consists of nearly spherical nanoparticles with a mean diameter close to 7 nm and size distribution from 4 to 12 nm. The sample deposited using 100 pulses (Fig. 2b) is formed by isolated nanoparticles with bigger sizes, around 9 nm, and broader size distribution from 5 to 16 nm. For the sample prepared using 200 pulses, the mean diameter increases to 19 nm with a very broad size distribution from 12 to 28 nm (Fig. 2c). Finally, the deposit obtained with 300 laser pulses shows a quasi-percolated state in which nanostructures with a mean diameter of 21 nm and size distribution from 12 to 30 nm are observed in Fig. 2d. These results reveal that the Bismuth layers consist of nanostructures with variable sizes

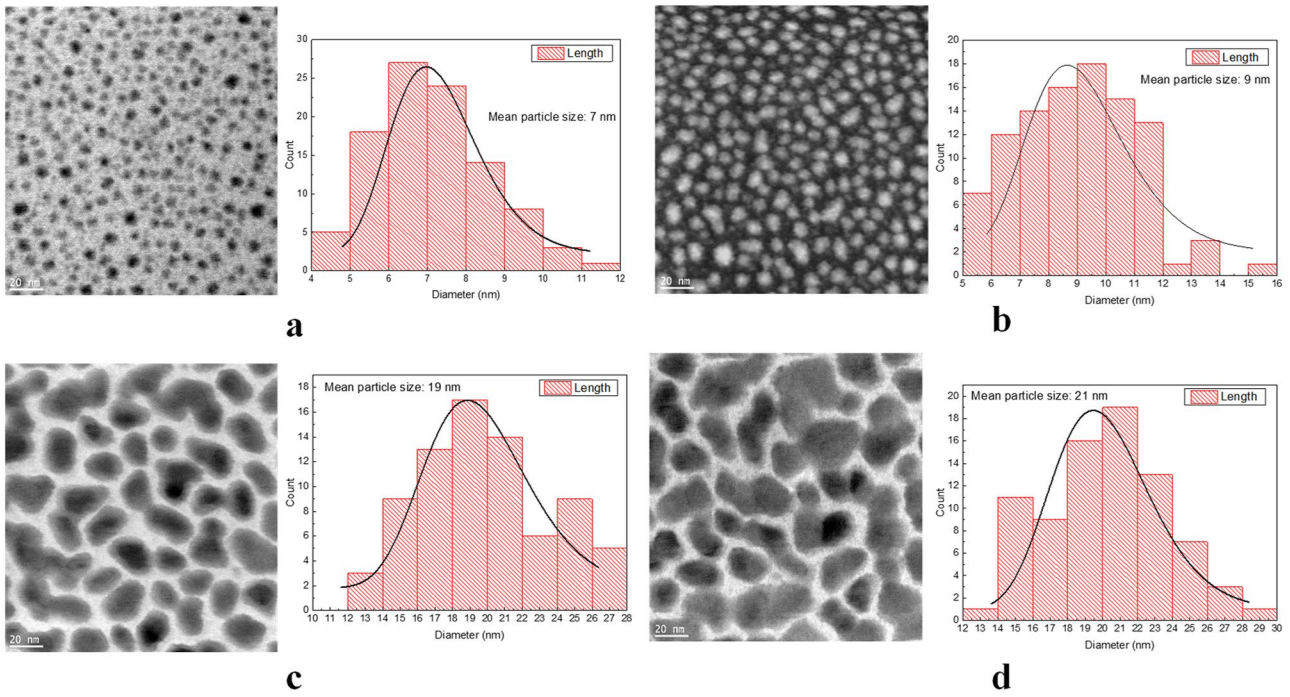

Fig. 2 Transmission electron microscopy (TEM) images of the Bi deposits at **a** 30, **b** 100, **c** 200, and **d** 300 laser pulses used to ablate the Bi target

and shapes depending on the number of laser pulses used to ablate the Bi target.

3.2 XPS characterization

Two XPS measurements were performed for all samples to determine the chemical bonding of the present elements (Ti, O, and Bi). The first one was done on the surface, whereas the second one was done after 30 s of etching time at the same point. In order to obtain information about the etching depth after 30 s, the sample deposited using 200 laser pulses on the Bi target was analyzed through a depth profile by XPS shown in Fig. 3. After 340 s of Ar^+ etching, the Si substrate is reached, with this data and the corresponding film thickness of 266 nm, a sputtering rate of approximately 0.78 nm/s is obtained. This results in an etching depth after 30 s close to 23 nm slightly thicker than the average thickness of the upper TiO_2 layer of 21 nm. Additionally, the XPS profile reveals a homogeneous distribution of Ti and O along the film thickness, the horizontal lines indicate the atomic concentration of Ti and O in TiO_2 in good agreement with the experimental data. The presence of the Bismuth layer was not evidenced probably due to the very low amount of this element. Another fact revealed from this compositional profile is the presence of a non-abrupt interface indicating a film-substrate interdiffusion.

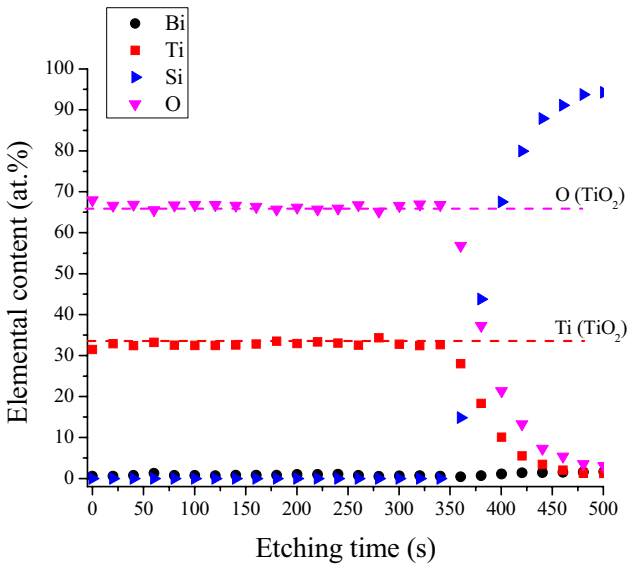

Fig. 3 XPS depth profile of the sample prepared using 200Bi pulses in S1 position

Figure 3 shows the XPS high-resolution spectra for the regions corresponding to Ti2p, O1s, and Bi4f of the samples deposited on substrate 1 (S1). Figure 4a shows the Ti2p region spectra of the sample without bismuth. The XPS spectrum acquired on the surface (black line) shows

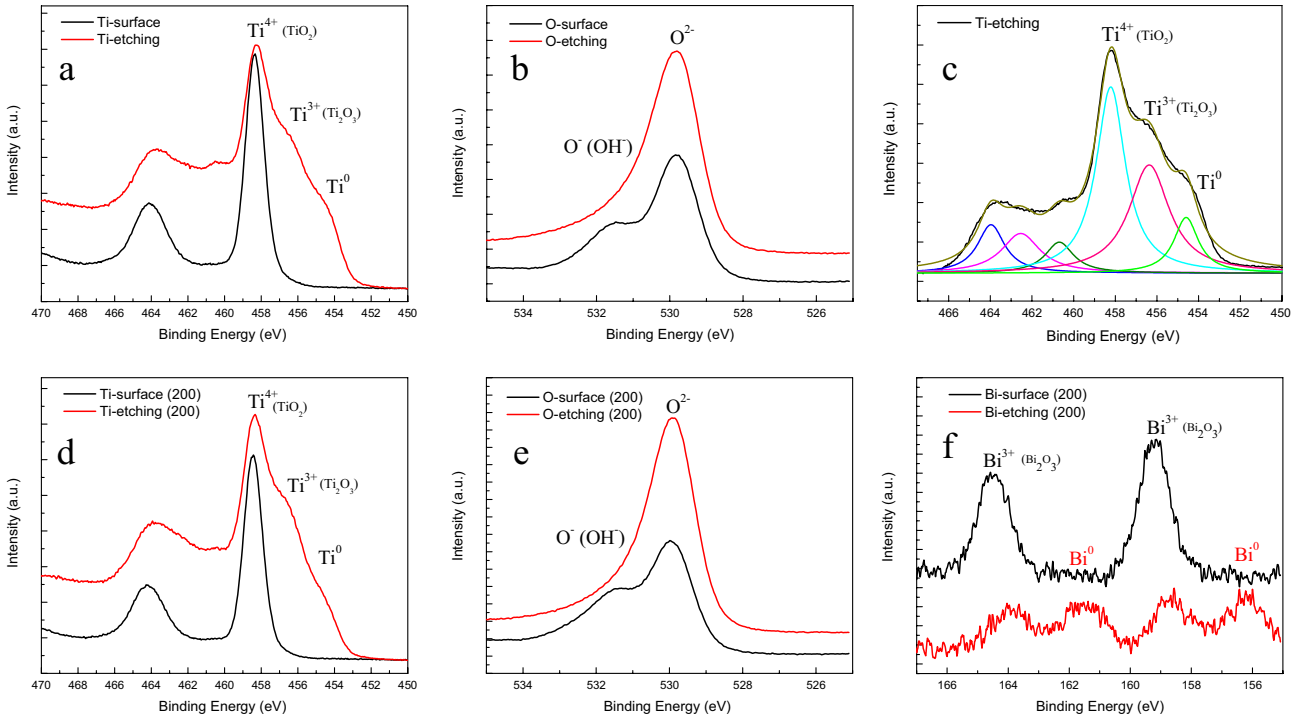

Fig. 4 XPS high-resolution spectra of the binding energy regions corresponding to **a** Ti2p, **b** O1s, and **c**Ti2p deconvolution of the sample without Bi and, **d** Ti2p, **e** O1s and **f** Bi4f zones for 200-Bi pulses sample in S1 position

a doublet with peaks at 464.1 and 458.3 eV corresponding to the $2p_{1/2}$ and $2p_{3/2}$ orbitals, respectively. Their position agrees well with Ti^{4+} in Ti–O bonds of TiO_2 [32]. After the etching, the 458.3 eV peak shows an asymmetric shape with at least two contributions of lower energy (red line), indicating the presence of different chemical states. Its deconvolution (Fig. 4c) shows the presence of two additional doublets with peaks at 456.4 and 462.5 eV for the first one and 454.5 and 460.7 eV for the second one. The first is attributed to Ti^{3+} in Ti_2O_3 [32], whereas the second is due to Ti^0 [33]. The presence of titanium with lower oxidation states could be ascribed to a chemical reduction effect due to preferential sputtering of O by the Ar ions used for etching, promoting the reduction of TiO_2 to Ti_2O_3 and metallic Ti [34, 35].

The high-resolution XPS spectra for the O1s region of the sample without bismuth (Fig. 4b) show asymmetric peak shapes with a tail to high energies. The spectra corresponding to the surface (black line) show a clear shoulder close to 531.5 eV attributed to O^- in surface hydroxyl (OH^-) due to adsorbed surface contaminants [36]. The spectrum acquired after 30 s of etching time (red line) practically does not show that signal confirming its surface nature. The most intense peak at 530.0 eV is attributed to O^{2-} species indicating the presence of TiO_2 [36]. Figures 4d, e shows the XPS spectra of the Ti and O regions, corresponding to the multilayer sample with deposits of 200 pulses of bismuth. Very similar behavior as described before for samples of pure TiO_2 is observed. It is worth mentioning that the XPS spectra of the Ti and O regions of all samples containing Bi show the same behavior. This result indicates that the titania layers are not affected due to the bismuth incorporation. Figure 4f shows the Bi4f XPS region of the multilayer sample with 200 pulses of bismuth by layer. The spectrum corresponding to the surface (black line) shows peaks at 159.1 and 164.8 corresponding to the $4f_{5/2}$ and $4f_{7/2}$ orbitals assigned to Bi^{3+} in Bi_2O_3 [37]. After etching (red line), additionally to these peaks, a doublet at 156.6 and 161.8 characteristics of Bi^0 [37] is observed. This result reveals that Bi is incorporated as a mixture of bismuth oxide and metallic bismuth as will be shown in the Raman characterization section.

Figure 5 shows the XPS spectra for the Ti2p, O1s, and Bi4f regions corresponding to the multilayers deposited on substrate 2 (S2). It is seen that the Ti2p and O1s regions (Figs. 5a–e) are almost identical to the spectra discussed previously for substrate 1 (S1), suggesting that TiO_2 is produced no matter the substrate position. Concerning the Bi signal (Fig. 5f) the same behavior is observed again with the only difference of a higher intensity indicative of a higher amount of bismuth incorporated on the substrate 2 (S2) due to the geometrical configuration since this substrate is closer to the bismuth target as shown in Fig. 1a.

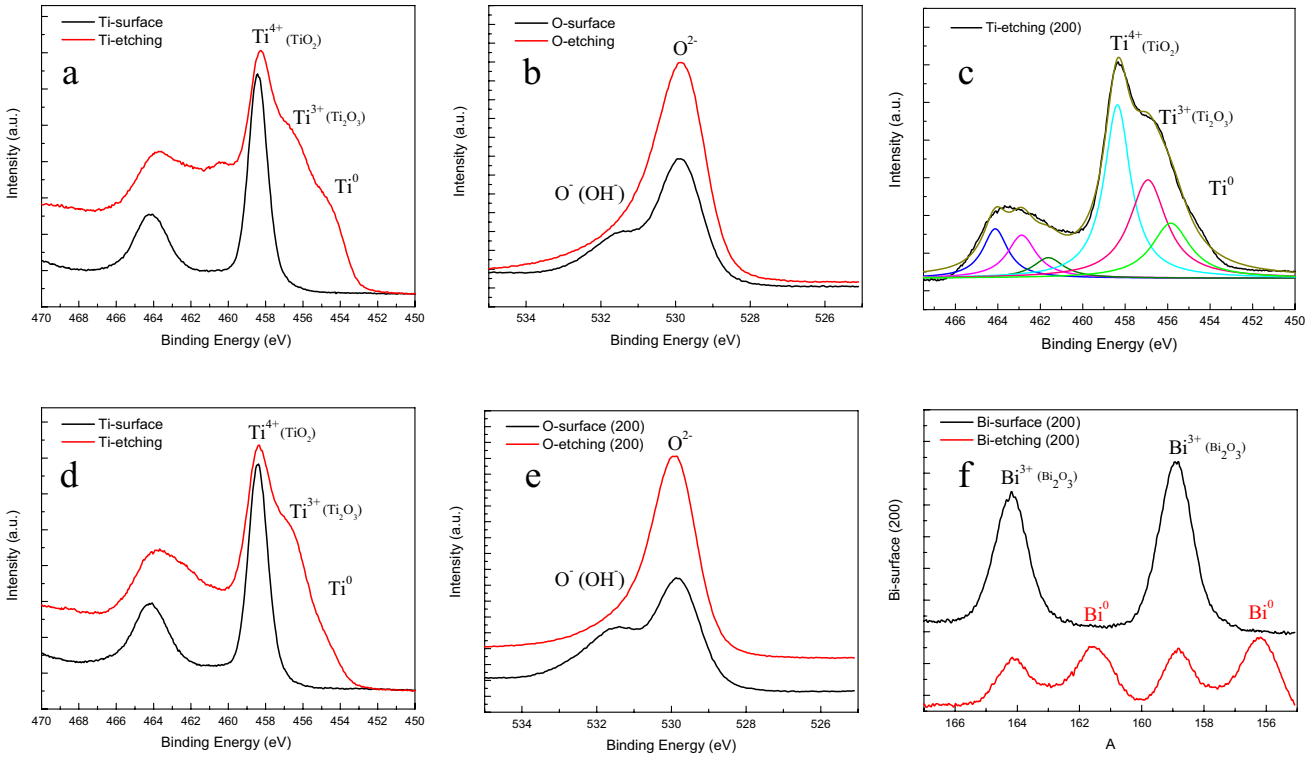

Fig. 5 XPS high-resolution spectra of the binding energy regions corresponding to **a** Ti2p, **b** O1s, and **c** Ti2p deconvolution of the sample without Bi and, **d** Ti2p, **e** O1s, and **f** Bi4f zones for 200-Bi pulses sample in S2 position

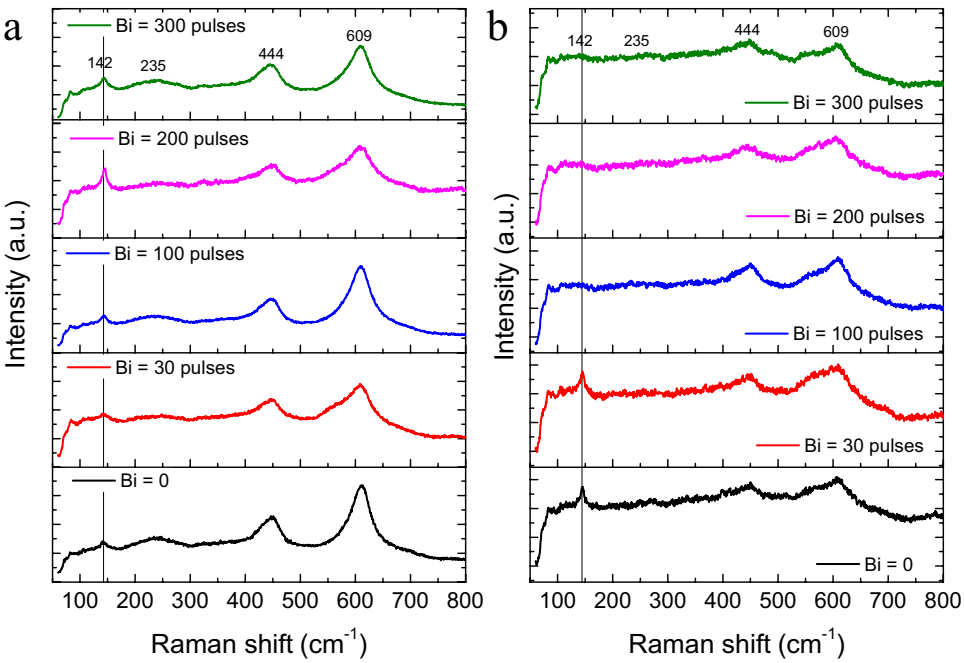

Fig. 6 Raman spectra of Bi/TiO_2 multilayers for substrate position **a** S1 and **b** S2

3.3 Microstructural characterization

Figures 6a, b shows the Raman spectra obtained for the films deposited on substrates S1 and S2, respectively. In general terms, these spectra show vibrational features at 142, 235, 444, and 609 cm^{-1} characteristics of the rutile phase [38]. These results indicate that the rutile phase is present in all the samples. Spectra shown in Fig. 6b, corresponding to

substrate 2, are less intense than those of the films deposited on substrate 1. This could be attributed to a lower thickness (as shown in Sect. 3.3) of these films due to a lower amount of Ti species arriving on substrate 2 in accordance with the geometrical setup as shown in Fig. 1a.

In order to gain insight into the microstructural features inside the films, the nanocomposite prepared using 300 pulses of Bi was scratched and Raman measurements were performed at several points on the detached material. Figure 7a shows a representative Raman spectrum of one of such measurements. In order to perform a detailed analysis, this spectrum was fitted with Lorentzian functions. The fitting results are shown in Figs. 7b, c where the Lorentzian functions corresponding to the Raman peaks are represented in different colors. These have their maximum at 72, 88, 95, 114, 124, 140, 229, 266, 314, 348, 403, 444, 512, 565, and 610 cm^{-1}. The peaks at 72 and 95 cm^{-1} are attributed to metallic Bi [39], the peaks at 140, 229, 444, and 610 cm^{-1} are attributed to titania in anatase–rutile mixture [38], and the peaks at 88, 114, 124, 266, 348, 403, 512, and 565 could be attributed to the α-Bi_2O_3 phase [40]. These results suggest that the nanocomposite is formed of a mixture of metallic bismuth, titania, and bismuth oxide, which is in good agreement with the XPS analysis.

3.4 Optical characterization

Transmittance measurements by UV–Visible spectroscopy were carried out to determine the bandgap energy, refractive index, and thickness of the nanocomposites. Figure 8 shows the transmittance spectra corresponding to the films deposited on substrates S1 (Fig. 8a) and S2 (Fig. 8b). The transmittance spectra are similar in both cases, indicating that the deposited materials have similar optical properties. A noticeable feature of these transmittance spectra is the presence of maxima and minima due to interference effects. The thickness and refractive index were determined using the Goodman model [41].

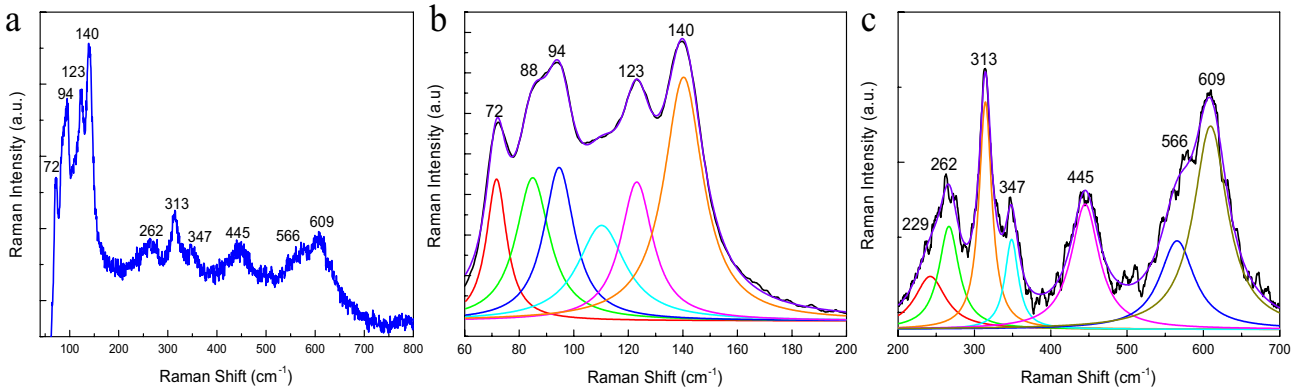

Fig. 7 Raman spectra of **a** multilayer prepared using 300 pulses on Bi for substrate position S2, **b**, and **c** its deconvolution in two different frequency regions

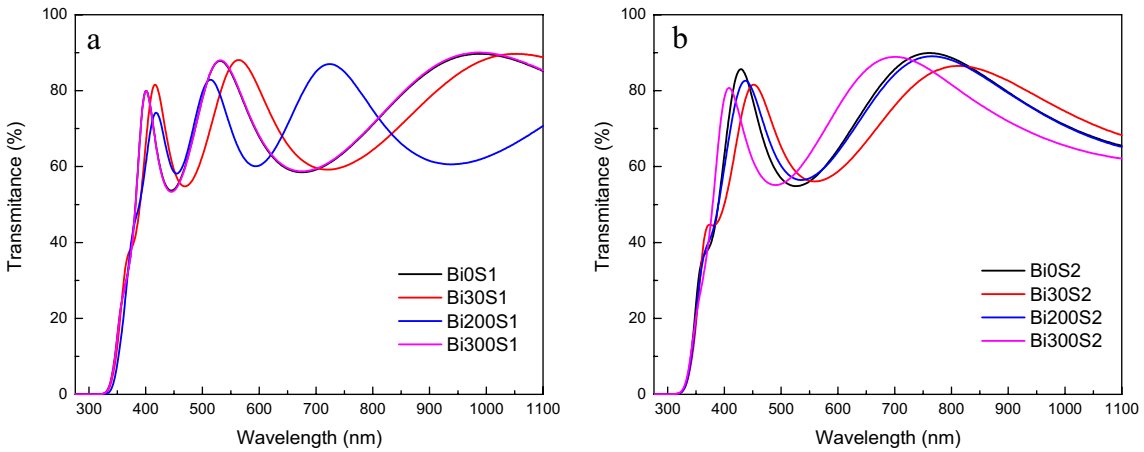

Fig. 8 Transmittance spectra of the Bi/TiO_2 multilayers for **a** S1 and **b** S2 substrate position

For films on substrate 1 (S1), the thicknesses were found from 254 to 266 nm, while thicknesses varied from 157 to 180 nm for substrate 2 (S2); these values correspond to mean deposition rates of 7.2×10^{-2} and 4.6×10^{-2} Å/pulse, respectively. That difference close to 40% is due to a higher titanium plasma density in the S1 position. Concerning the refraction index, for S1, its value varies from 2.4 to 2.7 and for S2 from 2.5 to 2.7 in both cases within the experimental uncertain. The bandgap energy (Eg) was determined using the Tauc method, assuming indirect transitions due to the nature of the semiconductor [42]. This was done by plotting $(\alpha h\nu)^{1/2}$ as a function of the photon energy. The optical absorption coefficient was obtained using the expression: $\alpha = -\ln(T)/t$, where t is the thickness of the film and T is the transmittance. The Eg values were obtained by a linear fit of the linear portion of the curve, determining its intersection with the photon energy axis as the quotient of the intercept to the slope. The values obtained from bandgap estimation were close to 3.2 eV for each thin film in accordance with the bandgap value of TiO_2.

Figure 9 shows the photoluminescence emission spectra obtained for the thin films deposited on both substrates. In general terms, it is observed that the spectra have the same shape for the films deposited on substrate S1 (Fig. 9a). Several PL features are observed at 396, 439, 451, 468, 484, and 493 nm. Emission at 396 nm is attributed to an interband transition corresponding to 3.1 eV in good agreement with the bandgap value determined from UV–Vis measurements. The signals at 451 and 468 nm are due to band edge-free excitons, whereas signals at 484 and 493 correspond to band excitons [43]. On the contrary, the PL emission for nanocomposites deposited on substrate S2 (Fig. 9b) shows important changes in the electronic structure of deposited materials in this position. These changes are probably related to the different deposition characteristics such as the kinetic energy and density of the plasma species impinging the substrate that depend strongly on their position in the chamber, additionally, differences in the density of the thin films are expected. Further studies are underway to find an explanation for this behavior which implies an extensive study of the luminescence properties of the thin films.

4 Conclusions

Bi/TiO_2 multilayer thin films were deposited on two substrates, placed at different positions, by a crossed beam pulsed laser deposition configuration. The characterization of the prepared multilayers indicates the presence of layers of crystalline TiO_2 in its rutile phase. The bismuth layers

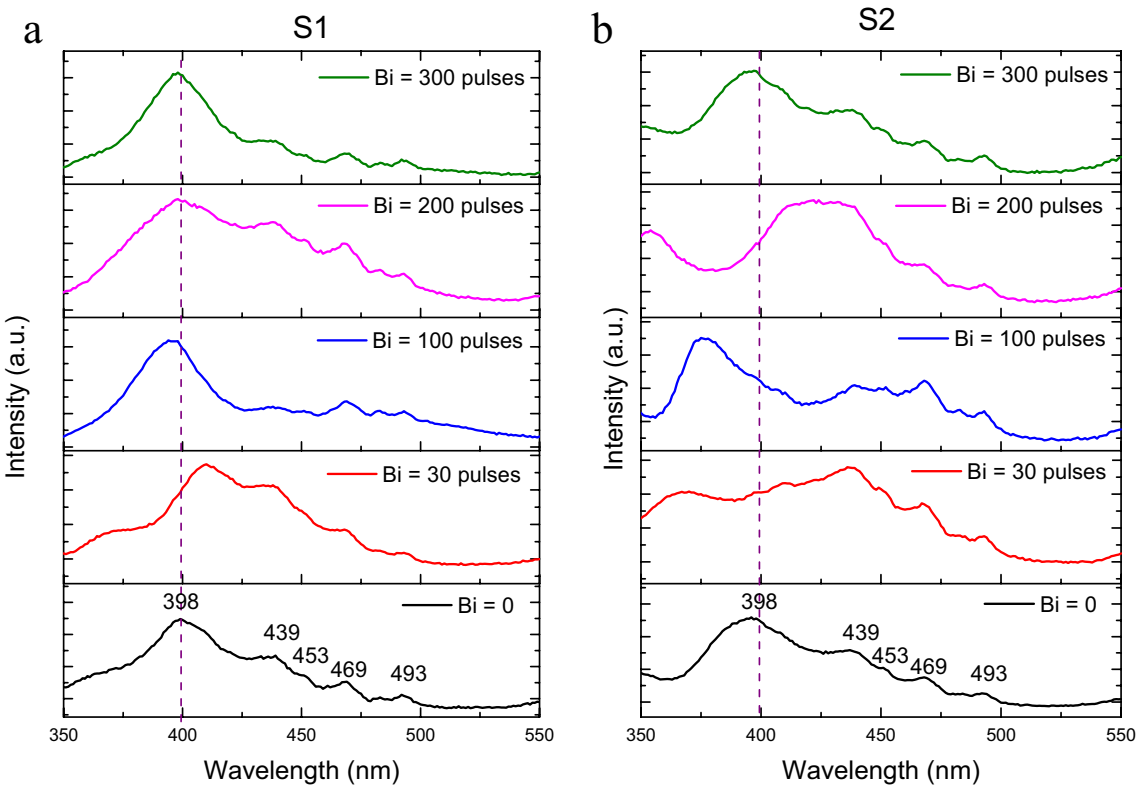

Fig. 9 Photoluminescence spectra for $TiO_2/Bi/TiO_2$ thin films

consist of bismuth nanostructures composed of mixtures of metallic Bi and Bi_2O_3. XPS results showed that the incorporation of Bi by this procedure does not affect the TiO_2 properties. The presence of Ti^{3+}, Ti^0, and Bi^0 species after the etching process is attributed to preferential sputtering of O leading to the reduction of Ti^{4+} to lower oxidation states. It was found that the thickness of thin films depends mainly on the substrate position and on the number of laser pulses used to ablate the Bi target. The PL emission changes drastically with the position of the substrate suggesting differences in the electronic structure for the S2 position.

Acknowledgments A. Martínez-Chávez thanks CONACyT for the scholarship granted (No. 815785). K. Esquivel and L. Escobar thank the Engineering Faculty-UAQ for the financial support granted through the Attention to national problems fund and the FONDEC-UAQ-2021. We greatly appreciate the collaboration of R. Basurto in performing the XPS measurements.

References

1. Fu. Yong-sheng, J. Li, J. Li, Nanomaterials **9**, 359 (2019)
2. D.K. Avasthi, Y.K. Mishra, R. Singhal, D. Kabiraj, S. Mohapatra, B. Mohanta, Nivedita K. Gohil, N. Singh, J. Nanosci. Nanotechnol. **10**, 2705 (2010)
3. Seishi Abe, Masato Ohnuma, De Hai Ping, Shigehiro Ohnuma, Appl. Phys. Express **1**, 095001 (2008)
4. M. Jiménez de Castro, R. Serna, M.G. Marzoa, A. Castelo, C.N. Afonso, E. Haro-Poniatowski, Appl. Surf. Sci. **257**, 5172 (2011)
5. R.S. Pedanekar, S.K. Shaikh, K.Y. Rajpure, Curr. Appl. Phys. **20**, 931 (2020)
6. Yu. Jia-Guo, Yu. Huo-Gen, B. Cheng, X.-J. Zhao, J.C. Yu, W.-K. Ho, J. Phys. Chem. B **107**, 13871 (2003)
7. Miguel Pelaez, Nicholas Nolan, Suresh Pillai, Michael Seery, Polycarpos Falaras, Athanassios Kontos, J. Patrick Dunlop, John Byrne Hamilton, Kevin O'Shea, Mohammad Entezari, Dionysios Dionysiou, Appl. Catalysis B Environ. **125**, 331 (2012)
8. Shama Rehman, A.M. Ruh Ullah, N.D. Gohar. Butt, J. Hazardous Mater. **170**, 560 (2009)
9. Schneider C.W., Lippert T. (2010) Laser Ablation and Thin Film Deposition. In: Schaaf P. (eds) Laser Processing of Materials. Springer Series in Materials Science, vol 139. Springer, Berlin, Heidelberg.
10. P.R. Willmott, J.R. Huber, Rev. Mod. Phys. **72**, 315 (2000)
11. A.A. Voevodin, M.A. Capano, A.J. Safriet, M.S. Donley, J.S. Zabinski, Appl. Phys. Lett. **69**, 188 (1996)
12. L. Escobar-Alarcón, F. Gonzalez-Zavala, D.A. Solis-Casados, M. Fernandez, J. Aspiazu, E. Haro-Poniatowski, Appl. Phys. A **124**, 358 (2018)
13. M. Jelinek, L. Bacakova, J. Remsa, T. Kocourek, J. Miksovsky, P. Pisarik, M. Vandrovcova, E. Filova, S. Kubinova, J. Mater. Sci. Chem. Eng. **4**, 98 (2016)
14. L. Escobar-Alarcón, D.A. Solis-Casados, S. Romero, E. Haro-Poniatowski, Appl. Phys. A **126**, 57 (2020)
15. J.G. Lunney, Appl. Surf. Sci. **86**, 79 (1995)
16. R. Serna, C.N. Afonso, C. Ricolleau, Y. Wang, Y. Zheng, M. Gandais, I. Vickridge, Appl. Phys. A **71**, 583 (2000)
17. M. Quintana, E. Haro-Poniatowski, J. Morales, N. Batina, Appl. Surf. Sci. **195**, 175 (2002)
18. Y.L. Wang, C. Chen, X.C. Ding, L.Z. Chu, Z.C. Deng, W.H. Liang, J.Z chen, G.S. Fu, , Laser Particle Beams **29**, 105 (2011)
19. S. Onari, M. Miura, K. Matsuishi, Appl. Surf. Sci. **197–198**, 615 (2002)
20. L. Escobar-Alarcón, J.G. Morales-Méndez, D.A. Solís-Casados, S. Romero, M. Fernández, E. Haro-Poniatowski, J. Phys. Conference Series **582**, 012013 (2015)
21. L. Escobar-Alarcón, J. Pérez-Álvarez, D.A. Solís-Casados, S. Enrique Camps, J. Jiménez-Becerril. Romero, Appl. Phys. A **110**, 909 (2013)
22. L. Escobar-Alarcón, D.A. Solís-Casados, S. Romero, J.G. Morales-Mendez, E. Haro-Poniatowski, Appl. Phys. A **117**, 31 (2014)
23. F. Gonzalez-Zavala, L. Escobar-Alarcón, D.A. Solís-Casados, S. Romero, M. Fernandez, E. Haro-Poniatowski, E. Rodríguez-Castellón, Catal. Today **305**, 102 (2018)
24. I. Olvera-Rodríguez, R. Hernández, A. Medel, C. Guzmán, L. Escobar-Alarcón, E. Brillas, I. Sirés, K. Esquivel, Sep. Purif. Technol. **224**, 189 (2019)
25. E. Haro-Poniatowski, M. Jouanne, J.F. Morhange, M. Kanehisa, R. Serna, C.N. Afonso, Phys. Rev. B **60**, 10080 (1999)
26. E. Haro-Poniatowski, R. Serna, M. Jiménez, A. de Castro, C.N. Suárez-García, Afonso and I Vickridge, , Nanotechnology **19**, 485708 (2008)
27. M. Jimenez de Castro, R. Serna, J. Toudert, J.M. Fernandez Navarro, E. Haro-Poniatowski, Ceramics Int. **41**, 8216 (2015)
28. L. Escobar-Alarcón, E. Haro-Poniatowski, M.A. Camacho-López, M. Fernández-Guasti, J. Jiménez-Jarquín y A. Sánchez-Pineda, , Appl. Surface Sci. **137**, 38 (1999)
29. L. Escobar-Alarcón, D.A. Solís-Casados, F. Gonzalez-Zavala, S. Romero, M. Fernandez, E. Haro-Poniatowski, J. Phys. Conference Series **792**, 012006 (2017)
30. B. Toftmann, J. Schou, T.N. Hansen, J.G. Lunney, Phys. Rev. Lett. **84**, 3998 (2000)
31. A.S. Bakri, M.Z. Sahdan, F. Adriyanto, N.A. Raship, N.D.M. Said, S.A. Abdullah, M.S. Rahim, AIP Conference Proc. **1788**, 030030 (2017)
32. J. Abad, O. Bohme, E. Román, Surf. Sci. **549**, 134 (2004)
33. B. Siemensmeyer, J.W. Schultze, Surf. Interface Anal. **16**, 309 (1990)
34. R. Simpson, R.G. White, J.F. Watts, M.A. Baker, Appl. Surf. Sci. **405**, 79 (2017)
35. G. Greczynski, L. Hultman, Appl. Surface Sci. **542**, 148599 (2021)
36. E. McCaterty, J.P. Wightman, Surf. Interface Anal. **26**, 549 (1998)
37. Housei Akazawa, Hiroshi Ando, Journal of Applied Physics **108**, 083704 (2010)
38. U. Balachandran, N.G. Eror, J. Solid State Chem. **42**, 276 (1982)
39. K. Trentelman, J. Raman Spectrosc. **40**, 585 (2009)
40. S.N. Narang, N.D. Patel, V.B. Kartha, J. Mol. Struct. **327**, 221 (1994)
41. A.M. Goodman, Appl. Opt. **17**, 2779 (1978)
42. J. Tauc, R. Grigorovici, A. Vancu, Phys. Status Solidi **15**, 627 (1966)
43. Feiyan Xu Haonan, Bei Cheng, Yu. Jiaguo, Wingkei Ho, Chem Cat Chem **11**, 6301 (2019)